# 3-D Eddy Current Torque Modeling

Subhra Paul, Walter Bomela and Jonathan Z. Bird

Laboratory for Electromechanical Energy Conversion and Control
University of North Carolina at Charlotte, NC 28223, USA

**This paper presents an analytic based eddy current torque analysis procedure. The equations are derived using the second order vector potential and the magnetic rotor is modeled using the magnetic charge sheet concept. The formulation enables the damping and stiffness equations to be derived. The equations are numerically computed and the accuracy is compared against experimental torque and power measurements.**

***Index Terms*— eddy currents, torque, Halbach rotor, maglev, second order vector potential.**

## I. Introduction

When a magnetic source moves in the vicinity of a conductive plate, time varying magnetic fields induce eddy currents in the plate which in turn interacts with the source magnetic field to create velocity dependent drag and lift force. The generated drag force can be utilized in applications such as eddy current braking [1] and rotor vibration damping [2]. While the lift force can be utilized to provide suspension for high-speed maglev trains [3]. Electrodynamic maglev suspension systems typically rely on a null-flux coil guideway topology in order to maximize the lift-to-drag ratio [4]. Another way to avoid this drag and achieve integrated suspension and propulsion for the vehicle at low cost is to rotate the magnetic source rather than translationally moving it above a conductive plate guideway. This electrodynamic wheel (EDW) concept is illustrated in Fig. 1(a) [5]. In order to create large lift force a flux-focusing Halbach rotor, as shown in Fig. 1(b), is used. In this approach the thrust force is dependent on the slip speed, $s_l$, defined as $s_l=\omega_m r_o - v_x$ where $\omega_m$, $r_o$ and $v_x$ are mechanical angular velocity, outer radius and translational velocity respectively.

Reitz and Davis [6] and later Langerholc [7] developed force and eddy current torque equations for a coil when there is only translational motion. This paper presents an analytic based eddy current torque, power, damping and stiffness analysis procedure for the case when a magnetic rotor is rotated and translationally moved above a conductive plate. The equations are derived using the second order vector potential[8-10] approach and the magnetic rotor is modeled using the magnetic charge sheet concept [11].

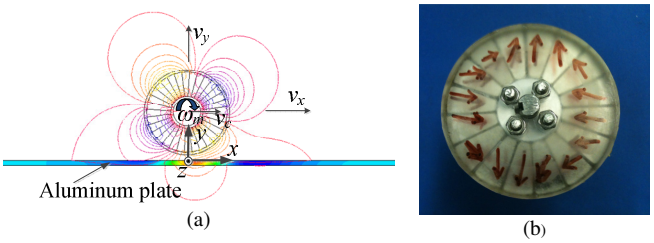


Fig. 1(a) A 2 pole-pair Halbach rotor rotating and translationally moving above an aluminum plate. Isoline plot of the reflected radial flux density and isosurface plot of the eddy current density is shown, (b) An experimental 2 pole-pair Halbach rotor with radial and shunt magnets

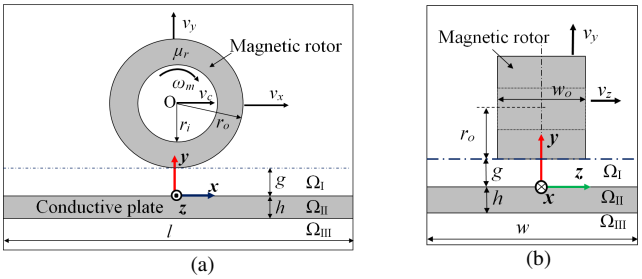


Fig. 2 The (a) *x*-*y* and (b) *z*-*y* view of the problem region.

## II. Governing Equations

A schematic showing the relevant problem regions is shown in Fig. 2. The rotor velocity in the *x*, *y* and *z* directions as well as rotational speed, $\omega_m$, is shown. The length, $l$ and width, $w$, of the plate are assumed to be large enough so that all fields are zero at the edges. The plate is assumed to have constant conductivity be nonmagnetic and simply connected.

### A. Conductive Region, $\Omega_{II}$

Utilizing the magnetic vector potential

$$\mathbf{B} = \nabla \times \mathbf{A} \tag{1}$$

the eddy current problems can be formulated as [8]

$$\nabla^2 \mathbf{A} = \mu_0 \sigma \frac{d\mathbf{A}}{dt} \tag{2}$$

where $\sigma$ = conductivity. Solving (2) leads to a solution procedure that is complicated due to the need to solve three scalar terms and also account for the coupling within the magnetic flux density components. This derivation complexity can be avoided by using the SOVP, **W**, defined as [9, 10]

$$\mathbf{A} = \nabla \times \mathbf{W} = \nabla \times [W_a \hat{y} + \hat{y} \times \nabla W_b] \tag{3}$$

where $W_a$ and $W_b$ are scalars. Only the transverse electric (TE) potential, $W_a$, is non-zero when solving eddy current problems in a conductive medium that is infinite in the *x*-*z* plane [9]. Therefore, the TE potential exists only normal to the conductive plate as illustrated in Fig. 3. The formulation in terms of TE enables one to think of eddy current problems in terms of reflected and transmitted field components [12]. Substituting (3) into (2) yields

$$\nabla^2 W_a = \mu_0 \sigma \frac{dW_a}{dt} \tag{4}$$

Utilizing the convective derivative

$$\frac{dW_a}{dt} = \frac{\partial W_a}{\partial t} + (\mathbf{v}\cdot\nabla)W_a \tag{5}$$

and assuming a steady state solution such that

$$W_a(x,y,z,t) = W_a(x,y,z)e^{-j(P\omega_m)t} \tag{6}$$

allows (4) to be written as

$$\nabla^2 W_a = -\mu_0\sigma\left(jP\omega_m W_a + v_x\frac{\partial W_a}{\partial x} + v_y\frac{\partial W_a}{\partial y} + v_z\frac{\partial W_a}{\partial z}\right) \tag{7}$$

where *P*=pole-pairs. Substituting (3) into (1) yields

$$\mathbf{B} = \frac{\partial^2 W_a}{\partial x\partial y}\hat{x} - \left(\frac{\partial^2 W_a}{\partial x^2} + \frac{\partial^2 W_a}{\partial z^2}\right)\hat{y} + \frac{\partial^2 W_a}{\partial z\partial y}\hat{z}\ ,\ \text{in } \Omega_{II} \tag{8}$$

### B. *Nonconductive Regions*, $\Omega_I$, $\Omega_{III}$

Since the conductivity is zero the governing equation is [13]

$$\nabla^2 W_a = 0\ ,\ \text{in } \Omega_I, \Omega_{III} \tag{9}$$

and the relationship to **B** simplifies to

$$\mathbf{B} = \nabla\left(\frac{\partial W_a}{\partial y}\right)\ ,\ \text{in } \Omega_I, \Omega_{III} \tag{10}$$

As the magnetic scalar potential, $\phi$, is defined as

$$\mathbf{B} = -\mu_0\nabla\phi \tag{11}$$

the magnetic scalar potential is related to the SOVP by

$$\phi = -\frac{1}{\mu_0}\frac{\partial W_a}{\partial y}\ ,\ \text{in } \Omega_I, \Omega_{III} \tag{12}$$

### C. *Boundary Conditions*

The continuity conditions in terms of the TE potential are [14]

$$W_a^s + W_a^r = W_a^{II}\ ,\ \text{at } y = 0 \tag{13}$$

$$\frac{\partial W_a^s}{\partial y} + \frac{\partial W_a^r}{\partial y} = \frac{\partial W_a^{II}}{\partial y}\ ,\ \text{at } y = 0 \tag{14}$$

$$W_a^{II} = W_a^{III}\ ,\ \text{at } y = -h \tag{15}$$

$$\frac{\partial W_a^{II}}{\partial y} = \frac{\partial W_a^{III}}{\partial y}\ ,\ \text{at } y = -h \tag{16}$$

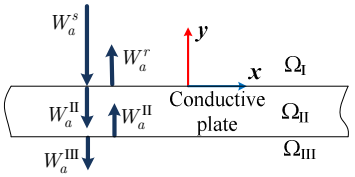


Fig. 3 The source, reflected and transmitted TE potentials.

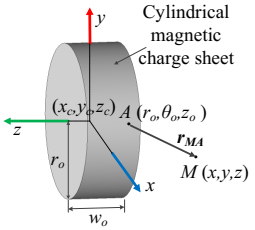


Fig. 4. Cylindrical magnetic charge sheet.

## III. General Solution

Applying the separation of variables method to (7) and (9) and noting that the field must decay when moving away from the conductive surface, the solution within each region is

$$W_a^r = \sum_{m=-\infty}^{\infty}\sum_{n=-\infty}^{\infty} C_{mn}^{I} e^{j\xi_m x}e^{jk_n z}e^{-\kappa_{mn}y} \tag{17}$$

$$W_a^{II} = \sum_{m=-\infty}^{\infty}\sum_{n=-\infty}^{\infty} [C_{mn}^{II}e^{\beta_{mn}y} + D_{mn}^{II}e^{-\beta_{mn}y}]e^{\lambda y}e^{j\xi_m x}e^{jk_n z} \tag{18}$$

$$W_a^{III} = \sum_{m=-\infty}^{\infty}\sum_{n=-\infty}^{\infty} C_{mn}^{III} e^{j\xi_m x}e^{jk_n z}e^{\kappa_{mn}(y+h)} \tag{19}$$

where

$$\xi_m = 2\pi m/l \tag{20}$$

$$k_n = 2\pi n/w \tag{21}$$

$$\beta_{mn}^2 = \lambda^2 + \gamma_{mn}^2 \tag{22}$$

$$\lambda = -0.5v_y\mu_0\sigma \tag{23}$$

$$\gamma_{mn}^2 = \kappa_{mn}^2 - \mu_0\sigma s_o \tag{24}$$

$$\kappa_{mn}^2 = \xi_m^2 + k_n^2 \tag{25}$$

$$s_o = j(Pw_m + \xi_m v_x + k_n v_z) \tag{26}$$

## IV. Source Field

In this paper the TE potential due to a Halbach magnetic rotor is calculated directly from the field created by an equivalent fictitious magnetic charge cylinder as shown in Fig. 4. The surface charge density on the cylinder is defined as [11]

$$\rho_{ms}(r_o,\theta_o,t) = 2B_r^s(r_o)e^{jP(\theta_o-\omega_m t)} \tag{27}$$

where

$$B_r^s(r) = \frac{2B_{rem}P(1+\mu_r)(r_i^{P+1} - r_o^{P+1})r_o^{2P}}{(1+P)[(1-\mu_r)^2 r_i^{2P} - (1+\mu_r)^2 r_o^{2P}]}\frac{1}{r^{P+1}} \tag{28}$$

is the Halbach rotor radial flux density [15]. $B_{rem}$= remanent flux density, $\mu_r$ = magnet relative permeability. The origin of the cylindrical charge sheet is located at $(x_c,y_c,z_c)$=(0,$r_o$+$g$,0). The scalar potential and magnetic flux density created by this charge cylinder at $y$=0 can be computed from [11]

$$\phi^{so}(x,y,z,t) = \frac{r_o}{4\pi\mu_0}\int_0^{2\pi}\int_{-w_o/2}^{w_o/2}\frac{\rho_{ms}(r_o,\theta_o,t)}{r_{MA}}dz_o d\theta_o \tag{29}$$

$$\mathbf{B}^{so}(x,y,z,t) = \frac{r_o}{4\pi}\int_0^{2\pi}\int_{-w_o/2}^{w_o/2}\frac{\rho_{ms}(r_o,\theta_o,t)}{r_{MA}^3}\mathbf{r}_{MA}dz_o d\theta_o \tag{30}$$

where

$$\mathbf{r}_{MA} = (x - r_o\cos\theta_o)\hat{x} + (y - y_c - r_o\sin\theta_o)\hat{y} + (z - z_o)\hat{z} \tag{31}$$

Utilizing (12) the source field in terms of the SOVP is

$$W_a^{so}(x,y,z,t) = -\frac{r_o}{4\pi}\int_0^{2\pi}\int_{-w_o/2}^{w_o/2}\left[\rho_{ms}(r_o,\theta_o,t)\right.$$
$$\left.\cdot\ln\left\{r_{MA} + (y - y_c - r_o\sin\theta_o)\right\}dz_o d\theta_o\right] \tag{32}$$

The integration with respect to $z_o$ is performed analytically whereas integration with respect to $\theta_o$ is accomplished numerically. In order to match the modes with the TE potentials given by (17)-(19), the source field, as given by (32) , is expressed as the following Fourier series within $\Omega_I$

$$W_a^s(x,y,z,t) = \sum_{m=-\infty}^{\infty}\sum_{n=-\infty}^{\infty}\frac{S_{mn}}{\kappa_{mn}^2}e^{j\xi_m x}e^{jk_n z}e^{\kappa_{mn}y}e^{-jP\omega_m t} \tag{33}$$

where the Fourier coefficients are determined from

$$S_{mn} = \frac{\kappa_{mn}^2}{lw}\int_{-w/2}^{w/2}\int_{-l/2}^{l/2} W_a^{so}(x,0,z,t)e^{-j\xi_m x}e^{-jk_n z}dxdz \tag{34}$$

Substituting (17)-(19), (33) into (13)-(16) and solving yields

$$W_a^r(x,y,z,t) = \sum_{m=-\infty}^{\infty}\sum_{n=-\infty}^{\infty} \frac{S_{mn}}{\kappa_{mn}^2} R_{mn}(y) e^{j\xi_m x} e^{jk_n z} e^{-jP\omega_m t} \quad (35)$$

where the reflection function, $R_{mn}(y)$, is

$$R_{mn}(y) = \frac{\mu_0\sigma[\kappa_{mn}v_y + s_o]}{2\kappa_{mn}^2 - \mu_0\sigma s_o + 2\kappa_{mn}\beta_{mn}\coth(\beta_{mn}h)} e^{-\kappa_{mn}y} \quad (36)$$

Substituting (35) into (12) and (10), the reflected scalar potential and magnetic flux density are

$$\phi^r(x,y,z,t) = \sum_{m=-\infty}^{\infty}\sum_{n=-\infty}^{\infty} S_{mn}\frac{R_{mn}(y)}{\mu_o\kappa_{mn}} e^{j\xi_m x} e^{jk_n z} e^{-jP\omega_m t} \quad (37)$$

$$\mathbf{B}^r(x,y,z,t) = \sum_{m=-\infty}^{\infty}\sum_{n=-\infty}^{\infty} e^{j\xi_m x} e^{jk_n z} e^{-jP\omega_m t} \left[ -j\frac{\xi_m}{\kappa_{mn}}\hat{x} + \hat{y} - j\frac{k_n}{\kappa_{mn}}\hat{z} \right] S_{mn} R_{mn}(y) \quad (38)$$

## V. Power, Torque, Stiffness and Damping

Within the nonconductive regions the fields are governed by magnetostatic equations, therefore the complex energy, $U_m$, can be computed from the magnetic charge [16, 17]

$$U_m = \frac{1}{2}\int_{-l/2}^{l/2}\int_{-w/2}^{w/2} \rho_{ms}^*(x,0,z,t)\phi^r(x,0,z,t)dxdz \quad \text{, at } y=0 \quad (39)$$

This enables the total energy to be determined from the interaction of the surface magnetic charge with the reflected field due to the eddy currents. For computation purposes it is most convenient to assume that the source magnetic charge is located on the surface of the conductive plate. In order to replicate the source field below the magnetic charge sheet the source charge density must be twice the normal component of the source magnetic flux density [11] which is

$$\rho_{ms}(x,0,z,t) = 2B_y^s(x,0,z,t) \text{ , at } y=0 \quad (40)$$

From (10) and (33) one obtains

$$\rho_{ms}(x,0,z,t) = 2\sum_{m=-\infty}^{\infty}\sum_{n=-\infty}^{\infty} S_{mn} e^{j\xi_m x} e^{jk_n z} e^{-jP\omega_m t} \quad (41)$$

The power is computed from the time derivative of (39)

$$P_{em} = \mathrm{Re}\left[\frac{\partial U_m}{\partial t}\right]_{\rho_{ms}(x,0,z,t)=\text{constant}} \quad (42)$$

$$P_{em} = \frac{lwP\omega_m}{\mu_0}\sum_{m=-\infty}^{\infty}\sum_{n=-\infty}^{\infty}\frac{|S_{mn}|^2}{\kappa_{mn}}\mathrm{Im}[R_{mn}(0)] \quad (43)$$

and the torque is then just

$$T_{em} = P_{em}/\omega_m \quad (44)$$

Using (44) the damping terms are

$$D_\theta = -\frac{\partial T_{em}}{\partial \omega_m} = -\frac{lwP}{\mu_0}\sum_{m=-\infty}^{\infty}\sum_{n=-\infty}^{\infty}\frac{|S_{mn}|^2}{\kappa_{mn}}\mathrm{Im}\left[\frac{\partial R_{mn}(0)}{\partial \omega_m}\right] \quad (45)$$

$$D_y = -\frac{\partial T_{em}}{\partial v_y} = -\frac{lwP}{\mu_0}\sum_{m=-\infty}^{\infty}\sum_{n=-\infty}^{\infty}\frac{|S_{mn}|^2}{\kappa_{mn}}\mathrm{Im}\left[\frac{\partial R_{mn}(0)}{\partial v_y}\right] \quad (46)$$

where the derivative terms are given by

$$\frac{\partial R_{mn}^w(0)}{\partial \omega_m} = \frac{j\mu_0\sigma P}{d_{mn}^2}\Big[d_{mn} + \mu_0\sigma\kappa_{mn}[\kappa_{mn}v_y + s_o]\coth(\beta_{mn}h)/\beta_{mn} + \mu_0\sigma[\kappa_{mn}v_y + s_o]\{1 - h\kappa_{mn}\mathrm{csch}^2(\beta_{mn}h)\}\Big] \quad (47)$$

$$\frac{\partial R_{mn}^w(0)}{\partial v_y} = \frac{\mu_0\sigma\kappa_{mn}}{d_{mn}^2}\Big[d_{mn} + \lambda[\kappa_{mn}v_y + s_o]\coth(\beta_{mn}h) \,/\, \beta_{mn} - \lambda h[\kappa_{mn}v_y + s_o]\mathrm{csch}^2(\beta_{mn}h)\Big] \quad (48)$$

and $$d_{mn} = \kappa_{mn}^2 + \gamma_{mn}^2 + 2\kappa_{mn}\beta_{mn}\coth(\beta_{mn}h) \quad (49)$$

Utilizing (39) the angular stiffness constant is obtained from

$$k_\theta = -\frac{\partial T_{em}}{\partial \theta} = -\frac{1}{\omega_m}\mathrm{Re}\left[\frac{\partial^2 U_m}{\partial t \partial \theta}\right]_{\rho_{ms}(x,0,z,t)=\text{constant}} \quad (50)$$

or, $$k_\theta = \frac{lwP^2}{\mu_0}\sum_{m=-\infty}^{\infty}\sum_{n=-\infty}^{\infty}\frac{|S_{mn}|^2}{\kappa_{mn}}\mathrm{Re}[R_{mn}(0)] \quad (51)$$

Similarly the vertical stiffness can be computed as

$$k_y = -\frac{\partial T_{em}}{\partial y} = \frac{lwP}{\mu_0}\sum_{m=-\infty}^{\infty}\sum_{n=-\infty}^{\infty}|S_{mn}|^2\,\mathrm{Im}[R_{mn}(0)] \quad (52)$$

TABLE I
Experimental Setup Parameters

| | Quantity | Value | Unit |
|---|---|---|---|
| Magnetic rotor | Outer radius, $r_o$ | 26 | mm |
| | Inner radius, $r_i$ | 9.6 | mm |
| | Width, $w_o$ | 52 | mm |
| | Remanent flux density, $B_{rem}$ | 1.42 | T |
| | Relative permeability, $\mu_r$ | 1.108 | - |
| | Pole pairs, $P$ | 2 | - |
| Conductive plate | Conductivity, $\sigma$ | $2.459\times10^7$ | S/m |
| | Width, $w$ | 77 | mm |
| | Outer radius | $600 \pm 0.58$ | mm |
| | Thickness, $h$ | 6.3 | mm |
| | Sheets separation | 101 | mm |

## VI. Experimental Results

An experimental vehicle setup with four EDWs has been constructed and is shown in Fig. 5-Fig. 6. The experimental parameters are given in Table I. In the setup the vehicle has been kept translationally stationary and the conductive plate on the guideway wheel is rotated to simulate translational motion, $v_x$. The EDWs are centered over the width of the conductive plate. The brushless dc motor torque and power are calculated using $T_{em}=K_tI_a$ and $P_{em}=K_tI_a\omega_m$ respectively where $K_t$=0.0295Nm/A. The current, $I_a$ and rotational speed, $\omega_m$, are measured using phase current and Hall Effect sensors. Laser displacement sensor is used to measure the air-gap, $g$.

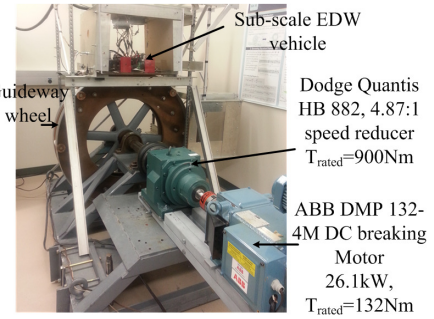


Fig. 5. Guideway wheel with an in-line gear reducer and DC braking motor.

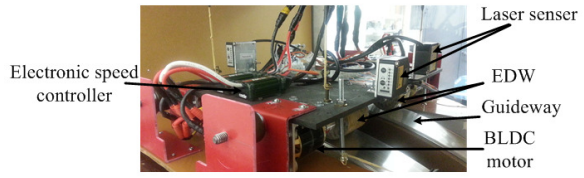


Fig. 6. Vehicle setup with four laser displacement sensors to measure air-gap

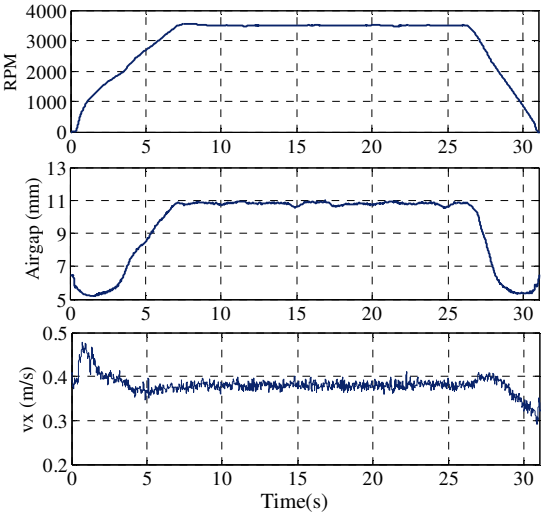


Fig. 7. RPM, airgap and translational velocity profiles of rear right EDW

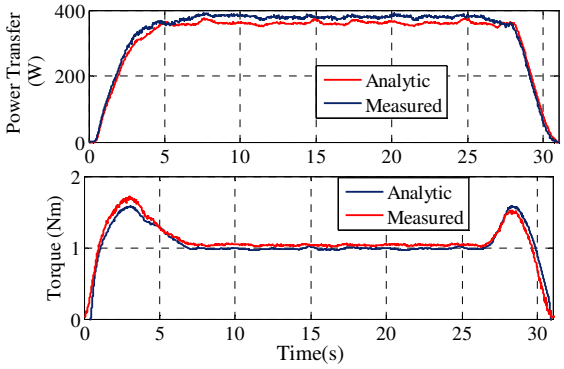


Fig. 8. Output power and torque comparison for rear right EDW

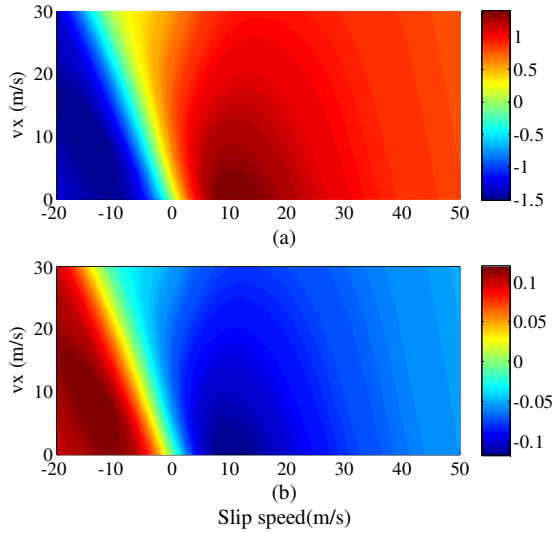


Fig. 9. (a) Torque (Nm) and (b) $D_y$ (Ns) as function of the translational velocity, $v_x$ and slip speed, $s_l$, for $(v_y,v_z)$=(0,0)m/s

The variation in rotational speed, air-gap and translational speed are shown in Fig. 7. The corresponding torque and power both measured and computed are shown in Fig. 8. An excellent agreement was obtained. Equations (43)-(44) were calculated using 31 harmonic components. The torque, vertical damping and stiffness terms as a function of translational velocity and slip speed are shown in Fig. 9-Fig. 10.

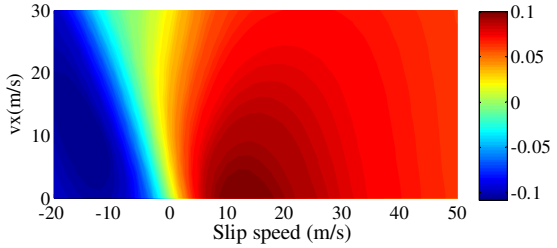


Fig. 10. $k_y$ (kN) as function of translational velocity, $v_x$ and slip speed, $s_l$, for $(v_y,v_z)$=(0,0) m/s

## VII. Conclusion

A 3-D analytic based steady-state eddy current torque, damping and stiffness equations have been derived using the SOVP formulation. The accuracy of the developed model has been validated against experimental results.

## References


[1] K. Lee and P. Kyihwan, "Modeling eddy currents with boundary conditions by using Coulomb's law and the method of images," *IEEE Trans. Magn.,* vol. 38, pp. 1333-1340, 2002.

[2] Y. Kligerman, O. Gottlieb, and M. S. Darlow, "Nonlinear Vibration of a Rotating System With an Electromagnetic Damper and a Cubic Restoring Force," *J. Vibration and Control,* vol. 4, pp. 131-144, 1998.

[3] H. Nakashima, "The superconducting magnet for the Maglev transport system," *IEEE Trans. Magn.,* vol. 30, pp. 1572-1578, 1994.

[4] K. R. Davey, "Designing with null flux coils," *IEEE Trans. Magn.,* vol. 33, pp. 4327-4334, 1997.

[5] J. Bird and T. A. Lipo, "Modeling the 3-D Rotational and Translational Motion of a Halbach Rotor Above a Split-Sheet Guideway," *IEEE Trans. Magn.,* vol. 45, pp. 3233-3242, 2009.

[6] J. R. Reitz and L. C. Davis, "Force on a Rectangular Coil Moving above a Conducting Slab " *J. Appl. Phys,* vol. 43, 1972.

[7] J. Langerholc, "Torques and forces on a moving coil due to eddy currents," *J. Appl. Phys,* vol. 44, 1973.

[8] W. R. Smythe, *Static & Dynamic Electricity*, 5th ed., 1989.

[9] T. P. Theodoulidis and E. E. Kriezis, "Impedance evaluation of rectangular coils for eddy current testing of planar media," *NDT & E Int.,* vol. 35, pp. 407-414, 2002.

[10] C. R. I. Emson, J. Simkin, and C. W. Trowbridge, "Further developments in three dimensional eddy current analysis," *IEEE Trans. Mag.,* vol. 21, pp. 2231-2234, 1985.

[11] S. Paul, D. Bobba, N. Paudel, and J. Z. Bird, "Source Field Modeling in Air Using Magnetic Charge Sheets," *IEEE Trans. Magn.,* vol. 48, pp. 3879-3882, 2012.

[12] Y. Li, T. Theodoulidis, and G. Y. Tian, "Magnetic field-based eddy-current modeling for multilayered specimens," *IEEE Trans. Mag.,* vol. 43, pp. 4010-4015, Nov. 2007.

[13] T. P. Theodoulidis and J. R. Bowler, "Eddy current coil interaction with a right-angled conductive wedge," *Proc. Roy. Soc. A,* vol. 461, pp. 3123-3139, October 8, 2005 2005.

[14] T. P. Theodoulidis, N. V. Kantartzis, T. D. Tsiboukis, and E. E. Kriezis, "Analytical and numerical solution of the eddy-current problem in spherical coordinates based on the second-order vector potential formulation," *IEEE Trans. Magn.,* vol. 33, pp. 2461-2472, 1997.

[15] Z. P. Xia, Z. Q. Zhu, and D. Howe, "Analytical magnetic field analysis of Halbach magnetized permanent-magnet machines," *IEEE Trans. Magn.,* vol. 40, pp. 1864-1872, 2004.

[16] E. P. Furlani, *Permanent magnet and electromechnaical devices materials, analysis, and applications*. San Diego: Academic Press, 2001.

[17] O. D. Jefimenko, *Electricity and Magnetism*. New York: Meredith Publishing Co., 1966.